Review article

Jie Liang, Haizhou Liu, Jianyu Yu, Lin Zhou* and Jia Zhu*

Plasmon-enhanced solar vapor generation

https://doi.org/10.1515/nanoph-2019-0039
Received February 9, 2019; revised March 30, 2019; accepted April 6, 2019

Abstract: Plasmonic nanostructures with strong light-matter interactions have been intensively explored in the past decades. The plasmonic photothermal effect has garnered significant research interest and triggered plenty of applications, such as photothermal therapy, photothermal imaging, and photocatalysis. Recently, plasmonic nanostructures are emerging as one of the most exciting candidates for solar vapor generation, inspiring the revival of solar-thermal-based water purification technologies. Here we present a review of state-of-the-art plasmonic-enhanced solar evaporation, including the theoretical background, various designs of plasmonic materials and structures, and their potential applications. The current challenges and future perspective are outlined as well.

Keywords: plasmonic nanostructures; broadband absorber; heat localization; photothermal; solar vapor generation; water purification.

1 Introduction

Plasmonic nanostructures have garnered tremendous attention from versatile research fields due to their unique capabilities to focus light into subwavelength volumes [1–6]. The basis of the well-known plasmonic effects [7, 8] is the high density of free electron gas (for noble metal ~10^{22} cm^{-3}) and the induced intrinsic collective oscillation of electrons. When excited by electromagnetic waves, the interactions between the free electrons and incident photons result in various plasmonic excitations, such as surface plasmon polaritons (SPP) [9], localized surface plasmon (LSP) [10] and hybridized plasmonic modes [5, 10, 11].

So far plasmonic effects have been intensively explored for subwavelength light sources [12], on-chip wave guiding [13, 14], color filtering [15, 16], molecular sensing [17, 18], photocatalysis [19, 20] and photovoltaics [21, 22]. Among most of the applications above, the intrinsic plasmonic photothermal effects [23–26], which dissipate the harvested photon energy into ohmic loss via electron participated scattering processes [27], have long been considered as an inevitably parasitic effect. On the other hand, the plasmon-based photothermal effect has been playing crucial roles in various fields, such as photothermal therapy [28–31], medicine delivery [32, 33], photothermal imaging [34], and material synthesis and assembly [35].

Very recently, an emergent plasmonic photothermal effect, plasmon-enhanced solar vapor generation (SVG), has triggered a revived research interest on an ancient solar water purification technology [36–40]. SVG is a natural photothermal phenomenon that induces liquid-vapor phase change of water by solar energy. As an essential part of the water cycle, the interaction of the Sun and the Earth (with >70% area covered by ocean) is endlessly providing purified water from seawater. However, such natural SVG process is rather inefficient (energy transfer efficiency <20%) because of the low solar energy harvesting capability as well as severe thermal losses. Plasmonic materials are promising candidates for enabling highly efficient SVG, due to enhanced light-matter interactions and electromagnetic fields in a tiny volume, beneficial for minimizing optical and thermal losses.

The plasmonic photothermal utilizations can be understood as follows. Surface plasmons, firstly known as collective electron oscillations in close proximity of the metal-dielectric interface [10, 20], can either propagate along the interface (SPP shown in Figure 1A) or be localized near the curved surfaces of metal nanoparticles (NPs) (localized surface plasmon resonance [LSPR] shown in Figure 1B) [10]. As shown in Figure 1C, the excited surface plasmons can behave as strongly damped oscillators [23,

***Corresponding authors: Lin Zhou and Jia Zhu,** National Laboratory of Solid State Microstructures, College of Engineering and Applied Sciences, School of Physics, Key Laboratory of Intelligent Optical Sensing and Integration, and Collaborative Innovation Center of Advanced Microstructures, Nanjing University, Nanjing, 210093, China, e-mail: linzhou@nju.edu.cn (L. Zhou); jiazhu@nju.edu.cn (J. Zhu)
Jie Liang, Haizhou Liu and Jianyu Yu: National Laboratory of Solid State Microstructures, College of Engineering and Applied Sciences, School of Physics, Key Laboratory of Intelligent Optical Sensing and Integration, and Collaborative Innovation Center of Advanced Microstructures, Nanjing University, Nanjing, 210093, China

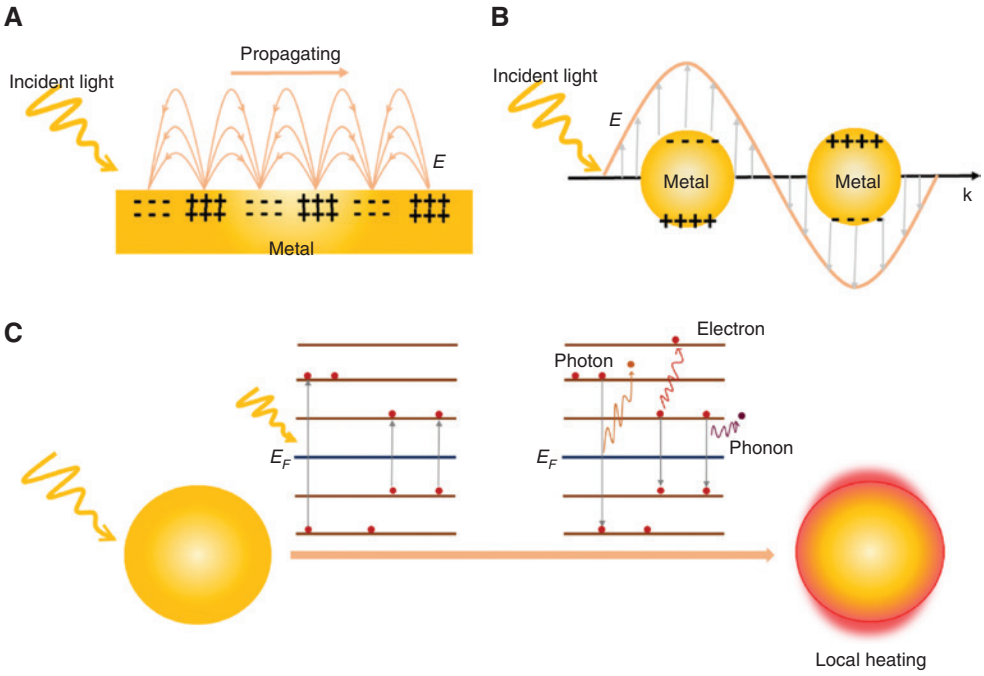

Figure 1: Schematics of the surface plasmons.
(A) Propagating surface plasmon generated (SPP) at the metal-dielectric interface; (B) localized surface plasmon resonance (LSPR) generated on the metal nanoparticles; (C) surface plasmon decays in three different ways (electron-to-photon, electron-to-electron, and electron-to-phonon) and ultimately generates local heating.

28, 41] and decay via different interplay channels (electron-to-photon, electron-to-electron, and electron-to-phonon), most of which are dissipated in the form of thermal energy [23, 24, 26].

Therefore, several common features are related to plasmonic nanostructures for solar thermal utilizations like SVG. Firstly, they are highly absorptive with various optical transition processes for the high density of free electrons [26, 42]. For example, metal-based plasmonic materials can fully utilize both interband and intraband transitions of optical absorption with low radiation recombination because of the unique band structure [43]. Thus, very thin plasmonic materials can enable strong light absorption. Secondly, the absorption spectra of plasmonic materials can be flexibly manipulated [42, 44–47], which can possess versatile optical modes [48–50], beneficial for ideal spectral matching with solar irradiance. Thirdly, surface plasmons can generate a pronounced local field enhancement up to thousands of times with respect to the incident field [10, 43, 51]. The energy of incident light is transformed into the oscillation energy of electrons and condensed electromagnetic field, which is ultimately converted into heat (called light-induced heat concentration) [3, 4, 24].

Plasmonic nanostructures enabled SVG not only features the effective light absorption and local heating conversion, but also provides platforms for investigations on intriguing microscopic mechanisms of photothermal processes. Pioneer works by Halas and co-workers [37, 38, 52] suggested the physical pictures of vapor generation and dynamics based on micro-spectroscopy. When gold NPs are excited at the LSP wavelength, the thin water layer around the NPs is heated locally due to resonant light absorption and ultrafast heat conversion, reaching or even exceeding the boiling point and transforming into nanobubbles (which gather to form a vapor shell). As the light illuminates continuously, the vapor shell gradually grows or coalesces and the buoyancy increases, with steam bubbles ascending toward the water surface and escaping. Note that, in this configuration, the microbubbles wrapped around metal NPs play crucial roles in light-induced local heating effect, which serve as thermal barriers and further reduce the thermal dissipation towards the bulk water. Another explanation is the Kapitza resistance induced by the vibrational energy mismatch between water molecules adsorbed on metal surfaces and those in bulk water [53], preventing vibrational energy transfer from the nanostructures into the surrounding water and thus increasing the solar vapor efficiency.

Here we present a brief review of recent progresses in plasmon-enhanced solar evaporation [26, 49, 54–64].

Diverse materials and structural designs for tuning the efficiency and bandwidth of light absorption and field enhancement are firstly discussed. Subsequently, a few typical strategies of plasmon-enhanced SVG are demonstrated. We finally discuss the current challenges and prospects in the future, aiming at inspiring further investigations at both the fundamental and applications levels.

2 Tailoring of plasmonic properties for light absorption

Ideal photothermal utilization of SVG requires both broadband light absorption over the solar spectrum in the far field and light-induced heat localization in the near field. The development of plasmonics and metamaterials has revealed that the resonant frequency and intensity of plasmon excitations are strongly dependent on the intrinsic material properties [10, 65], including sizes [37, 66], shapes [48, 67], surrounding environment [10, 20, 68], and assembly profiles [20, 69]. Figure 2 summarizes some primary factors that can contribute to the tunability of absorption spectra [37, 69, 70] as well asthe enhancement of localized electromagnetic fields [51, 65, 68].

Figure 2A–C shows representative structure-induced manipulation of the LSP resonant wavelength, which plays a crucial role in broadening the absorption bandwidth. Sizes of plasmonic NPs can lead to a resonant peak shift or a broadening of the absorption spectra [71, 72]. As shown in Figure 2A, Halas et al. reported that Au NPs with different diameters have different LSPR peak shifts [37]. On account of the damping and dephasing effects of surface oscillation, the broadening and absorptive dissipation of the surface plasmon are largely determined by the imaginary part of the dielectric constant [20, 73–75].

Light absorption in plasmonic NPs is also sensitive to the presence of adjacent NPs due to the plasmonic hybridization effect [69, 76–80]. When two metal NPs are adjacent to each other, their plasmon resonance modes will be coupled through near-field interactions, which can further lead to spectral splitting and plasmonic Fano resonance [76–80]. Hentschel et al. explored the extinction spectra of an isolated gold particle, gold monomer, gold hexamer, and gold heptamers with different interparticle gaps, as shown in Figure 2B [69]. Dipolar plasmon resonances were observed in the gold monomer and hexamer. In different heptamers, the transition from isolated to coupled modes is obvious when decreasing the interparticle gap. Specifically, when the interparticle gap distance is below 60 nm, a pronounced Fano resonance is formed with distinct resonance dips because of the destructive interference between the narrow subradiant mode and the broad superradiant mode.

Apart from plasmon hybridization, particle shape is another crucial aspect to tune the bandwidth of absorption [67, 70]. For example, Benjamin et al. calculated the absorption spectra of silver NPs (with the same size but various shapes) according to Mie theory (Figure 2C) [67]. It was clearly demonstrated that NPs with higher symmetry, such as spheres, cubes and triangular plates, have stronger absorption peaks. The plasmonic resonant wavelength varies from 400 to 800 nm, associated with the accumulation of surface charges at sharp corners also known as hot spots. On the contrary, the octahedron and the tetrahedron particles with lower symmetry have much broader but weaker absorption peaks with multiple resonances. Therefore, reducing the shape symmetry of plasmonic NPs is an effective method of broadening the spectra band.

In addition to efficient and tunable light absorption, the local electromagnetic field enhancement around metal/dielectric interface is another key factor influencing the photothermal effect [10, 43, 51], which is dependent on materials, geometries, and dielectric environment of the plasmonic structures (Figure 2D–F). To evaluate the enhancement of near-field effect that contributes to plasmonic photothermal processes, a dimensionless enhancement factor E_F is widely employed for simplicity [65], which is defined as the square of the ratio of the maximal electric field amplitude in the vicinity of NPs (E_{max}) and the incident electric field (E_0) ($E_F = |E_{max}/E_0|^2$). E_F is highly dependent on types of plasmonic materials and particle geometry as well as dielectric response of environmental materials, etc.

The development of plasmonic field has evidenced several factors that play crucial roles in the tuning of E_F [10, 20]. Guillaume Baffou et al. illustrated that, for a fixed dipolar sphere structure configuration, different metals show quite different near-field enhancement (Figure 2D) [65]. Noble plasmonic metals, such as gold, possess more pronounced near-field enhancement than Cu and Ta. Interestingly, some non-metal-based plasmonic materials were predicted with higher enhancement factor up to 28, mainly due to an even higher $|\varepsilon'/\varepsilon''|$ (the ratio of the real part and the imaginary part of the permittivity of the material).

Apart from the material choice of metals, different geometries of metal NPs can result in different field enhancements. Taking Au NPs for example, Figure 2E shows the calculated field enhancement difference induced by spheres (100 nm in diameter) and triangle

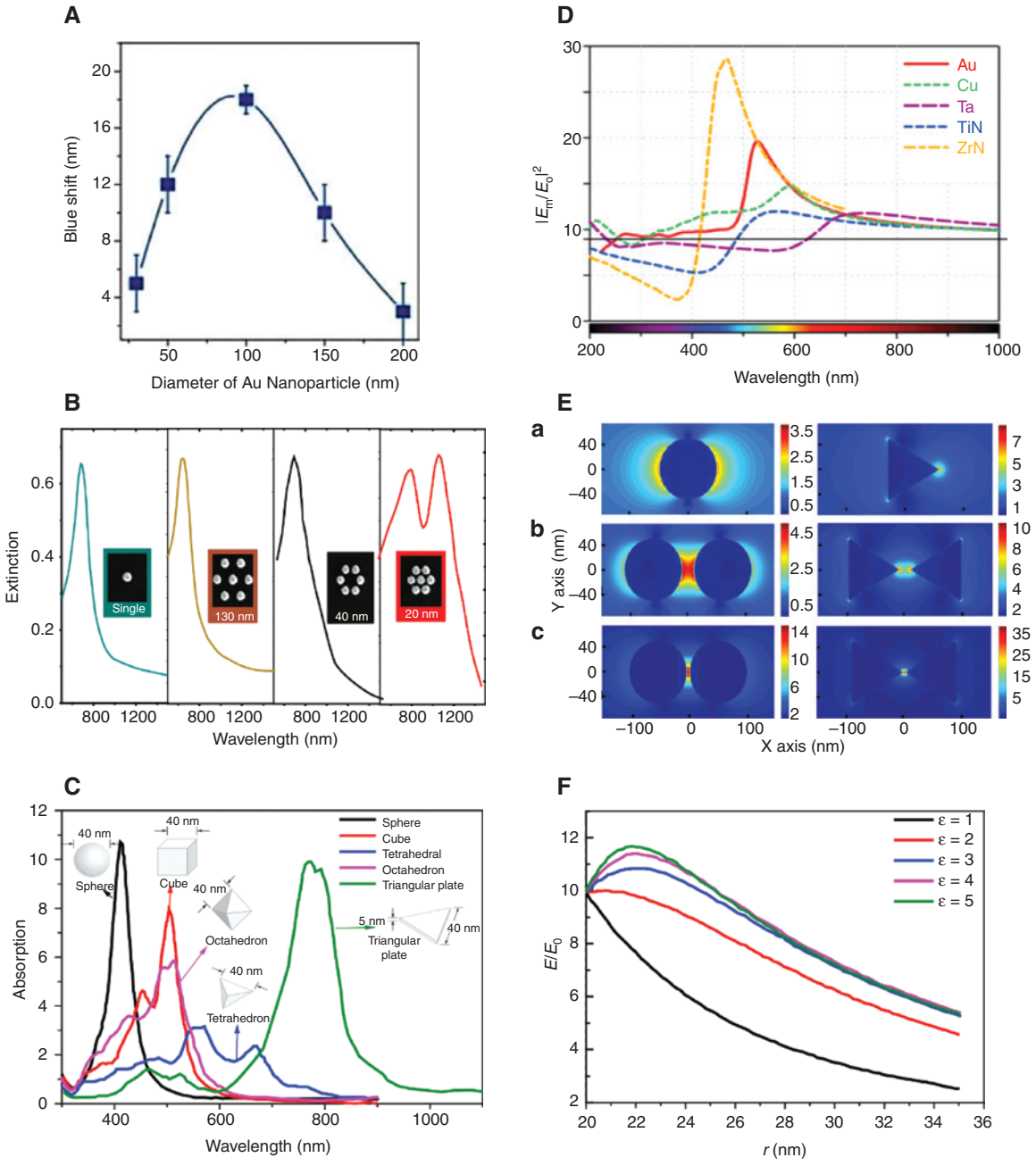

Figure 2: Absorption bandwidth and localized electromagnetic field enhancement.
The dependence of absorption spectra of plasmonic materials on (A) size for the same Au spherical shape [37], (B) assembly [69], and (C) shape [67]; the dependence of near electromagnetic field enhancement on (D) materials [65], (E) geometry (Au nanosphere of 100 nm diameter [left] and nanotriangle plate of 100 nm side length and 20 nm height [right] excited by monochromatic light [785 nm], [a] is the single nanoparticle system, [b] and [c] are two nanoparticle systems with gaps of 20 nm and 5 nm, respectively); (F) dielectric surroundings [68], respectively. (A) Reprinted with permission from Ref. [37]. Copyright 2013 American Chemical Society. (B) Reprinted with permission from Ref. [69]. Copyright 2010 American Chemical Society. (C) Adapted with permission from Ref. [67]. Copyright 2007 American Chemical Society. (D) Reprinted with permission from Ref. [65]. Copyright 2015 American Chemical Society. (F) Adapted by permission from Ref. [68].

plates (100 nm in side length and 20 nm in height) excited by monochromatic light (785 nm). One may find that NPs with sharper corners (like triangles) can generate higher local field enhancement than isotropic smooth particles, similar to those observed in heterogeneous systems [10, 20, 43, 51]. In addition, larger field enhancement can be suggested by close packed particles assembled with decreasing intergaps (Figure 2E [b and c]).

Dielectric environment is a third parameter for manipulating both plasmonic resonant wavelength and field enhancement [10, 20, 68]. Zhao et al. calculated the field enhancement of bimetallic nanocore/shells (the inner gold core with a radius of 5 nm and the silver shell with a thickness of 15 nm) as a function of dielectric coating thickness as well as dielectric constant of surroundings [68]. As illustrated in Figure 2F, for an arbitrary NP with fixed geometry parameters, the field enhancement factor increases with the dielectric constant of the surrounding media ε. When excited by incident electromagnetic field, free electrons on the surface of metal NPs induce polarization charges in the surrounding materials, which is highly adjustable by changing the dielectric constant of the surroundings. Therefore, increasing the amount of the induced polarization charges with an increased dielectric constant can enhance the dielectric screening of the Coulombic restoring force, beneficial for the electric field enhancement. On the other hand, the electric field decreases as the thickness increases for a fixed dielectric surrounding media. The nonmonotonic field enhancement as a function of thickness (especially for larger dielectric constant) can be ascribed to the synergetic contributions of dielectric constant and thickness.

Note that both the absorption bandwidth and localized electromagnetic field enhancement in Figure 2 can be flexibly tailored by materials and structure designs. Therefore, plasmonic nanostructures with fine chosen materials and well-defined structures can be ideal candidates for high-efficiency SVG by simultaneously tuning the absorption spectrum and field enhancement.

3 Plasmon-enhanced solar evaporation

The plasmonic materials-enabled solar evaporation process can be divided into three subprocesses: solar energy harvesting by plasmonic resonant absorption, light-to-heat conversion via electron relaxation, and heat transfer to water as latent heat via phonon scattering. In order to realize highly efficient solar evaporation, light absorption and light-to-heat conversion are two major processes most deeply investigated thus far, and the overall vapor generation efficiency can be expressed as the product of light absorption efficiency and light-to-heat conversion efficiency [81]:

$$\eta = \frac{AP_{\text{abs}}}{AP_{\text{solar}}} \cdot \frac{mh_{LV}}{AP_{\text{abs}}} \quad (1)$$

The first term on the right refers to the light absorption capability, where AP_{solar} and AP_{abs} refer to incident and absorbed solar power, respectively. The second term stands for light-to-heat conversion, m and h_{LV} being the mass of evaporated water and enthalpy change, respectively. Plasmonic materials interact strongly with the incident light at the resonant frequency, which greatly enhances the incident light absorption [26, 42]. However, the sunlight possesses not only low power density (1000 W/m^2 for ideal AM [air mass coefficient] 1.5 G solar illumination), but also a broad distribution in 280–4000 nm (~99% of which is in the range of 400–2500 nm) [82]. Therefore, it is necessary to artificially manipulate the absorption bandwidth so as to match the solar irradiance spectrum regime. In this part, we will discuss some recent representative efforts to enhance the light absorption and light-to-heat conversion efficiency with respect to the broadband characteristics of solar irradiance.

3.1 Plasmon-enhanced absorption for solar evaporation

In order to improve the solar evaporation efficiency, the input solar energy should be effectively harvested by plasmonic nanostructures. Therefore, broadband plasmonic solar absorbers are highly desired. As overviewed above, surface plasmon resonances are strongly affected by material [10, 65], size [37, 66], shape [48, 67], surrounding environment [10, 20, 68] and assembling profiles [20, 69], resulting in efficient absorption in particular wavelength range. Noble metals such as Au and Ag have been extensively investigated in the field of solar energy conversion, due to their strong visible and infrared (IR) plasmonic responses [17, 83, 84], which are well matched with the solar spectrum. In the past few years, many other metals have attracted much attention in this field as well, such as Al, Cu, Mo, Co, Ni, Pt, Pb, Ti, W, and Te [50, 65, 85–87]. There have been significant efforts to achieve a broadband and efficient absorption through plasmonic hybridization between different building blocks [17, 42, 47, 52, 61].

In 2013, the Halas group reported the first plasmon-assisted solar evaporation, which has inspired the exciting development in the following 5 years [52]. As shown in Figure 3A, they dispersed SiO_2/Au NPs in water to enhance the evaporation process. These NPs possess a SiO_2 core of 120 nm in diameter and a gold nanoshell of 40 nm in thickness. The plasmons associated with the inner and outer surfaces of the shell mix and hybridize. They found that hybridization interaction is stronger for thinner shell layers, leading to a strongly red-shifted resonance

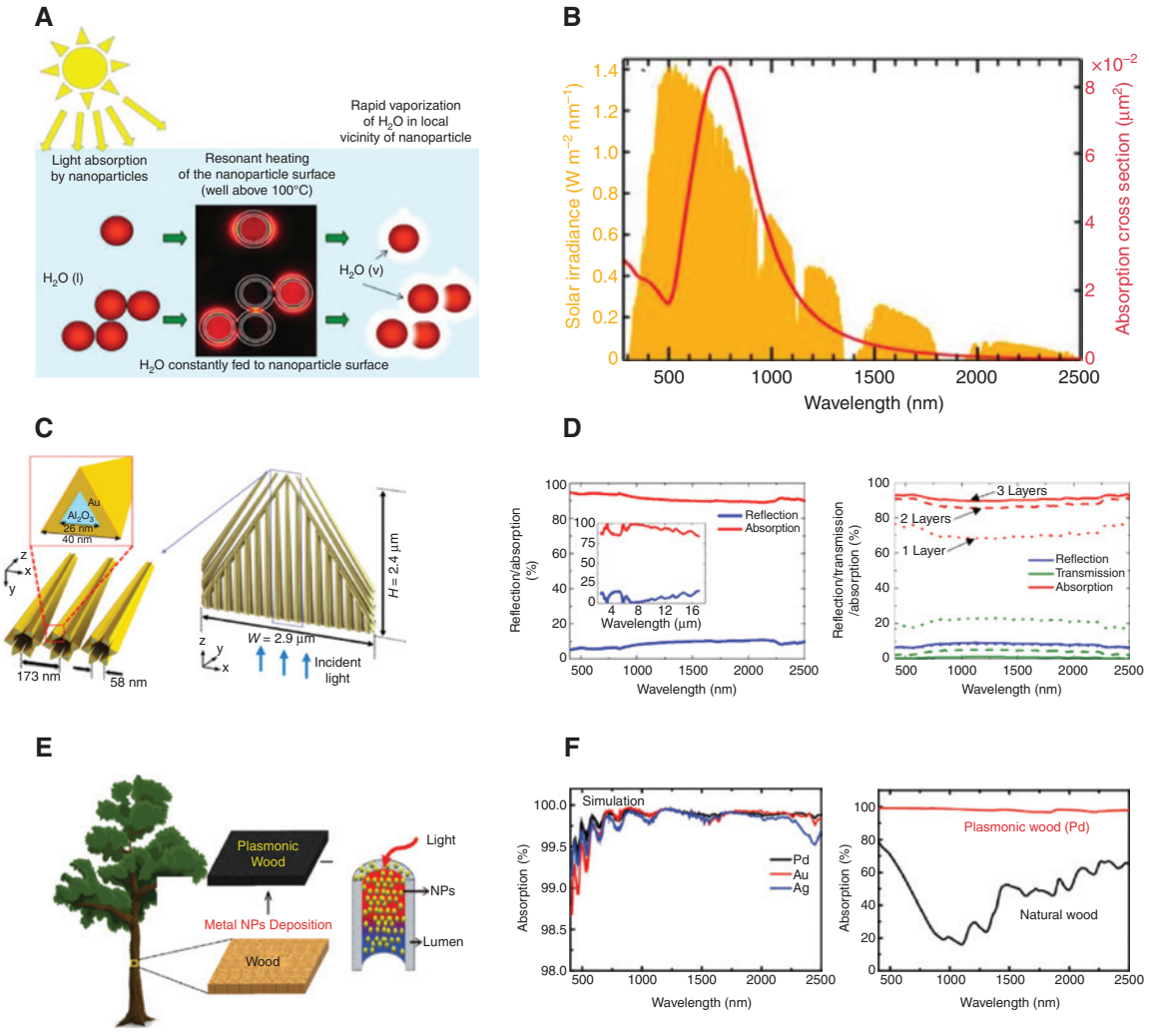

Figure 3: Highly integrated plasmonic structures to achieve high and broadband solar absorption.
(A) SiO_2/Au nanoshells structure and (B) the relative absorption cross section which overlaps the solar spectrum [52]; (C) schematic of flexible thin-film black gold membrane consisting of self-aggregated metallic nanowire bundle arrays and (D) the optical properties of single layer (left) and multilayer membrane (right) [88]; (E) schematic of plasmonic wood and (F) its enhanced absorption performance [59]. (A) and (B) Reprinted with permission from Ref. [52]. Copyright 2013 American Chemical Society. (C) and (D) Reprinted with permission from Ref. [88]. Copyright 2016, Nature Publishing Group. (E) and (F) Reprinted with permission from Ref. [59]. Copyright 2014 American Chemical Society.

for the "bright" plasmon at a wavelength determined by the thickness of the shell and the overall particle radius [27]. Because of plasmon hybridization, the plasmon resonance-induced absorption cross section is tuned to overlap with the solar spectrum (Figure 3B).

The past few years evidenced explosive developments of plasmonic solar evaporators with various broadband light harvesting structures. Marcin S. Zielinski et al. demonstrated a special technique to fabricate Ag/Au bimetallic hollow mesoporous plasmonic nanoshells as an efficient material for solar evaporation to produce vapor at high rates [89]. It was shown that for the 5 nm hollow Ag/Au alloy shells, the reported absorption peak was ~1280 nm. Although it is far from the irradiant peak of the solar spectrum (~500 nm for 5800 K blackbody irradiance), the utilized broadband region of the solar spectrum in the near-IR (NIR) regime was still enough to enhance the water vaporization efficiency, provided that the plasmonic nanostructures are carefully designed. The vapor generation kinetics is significantly improved due to the NP architecture, surface stabilization with a short PEG ligand, improved buoyancy, and material composition.

Apart from the core/shell structure, there are a couple of more idealized structures for polarization-independent broadband light absorption [59, 60, 85, 88]. Kyuyoung Bae et al. developed one large-area flexible thin-film black

gold membrane consisting of self-aggregated metallic nanowire bundle arrays, which incorporated adiabatic nanofocusing to reach an average absorption of 91% at 400–2500 nm [88]. This membrane was fabricated by self-aggregation of collapsed nanowires after appropriate pore widening of the anodic aluminum oxide (AAO), then sputtered with gold film of 40 nm thickness. The unit of the nanowires structure was shaped like the star of David with a triangular cross section of each nanowire. Then these hexagonal units merge and align to a funnel-shaped bundle as shown in Figure 3C. Both the small taper angles and gradually changed nanogaps between the aggregated nanowires are proven as contributions to broadband absorption in the visible and NIR regions. Figure 3D shows their experimental measurement of total reflection, transmission, and absorption spectra for the black gold membrane on an aluminum tape.

Incorporation of other 3D porous matrices with plasmonic NPs also performs an appreciably enhanced solar absorption. Natural wood has attracted much attention of researchers owing to its naturally mesoporous and hierarchical structure [90–92]. Uniform deposition of plasmonic metal NPs (Pb, Au, and Ag) into the natural wood pores led to the preparation of plasmonic wood by the Hu group [59], which turned black as illustrated in Figure 3E. Ultimately, due to the plasmonic effect of the metal NPs and the waveguide effect of the wood microchannels, the plasmonic wood was reported to have a highly enhanced light absorption ability (~99%) over 200–2500 nm wavelength range (plotted in Figure 3F). In addition, because of the multiple scattering and the absorption of the special microstructures in the wood, the efficient absorption was angle-independent. As a result, the naturally hydrophilic plasmonic wood with numerous microchannels for water transport performed impressive high-efficiency solar evaporation.

Among various articles about plasmonic evaporators (utilizing plasmonic materials) reported thus far, the Zhu group reported a series of three-dimensional plasmonic NPs for solar evaporation in 2016, as illustrated in Figure 4 [60, 85]. Unlike the conventional designs for plasmonic absorbers which commonly employ flat optical substrates [49, 93], they employed a three-dimensional nanoporous substrate as the scaffold of the solar evaporator. Such porous substrate is ideal for solar evaporation with three advantages. Firstly, the porous substrate greatly changes the distribution profile of the metallic NPs, from a continuous metal film to well-defined close-packed three-dimensional NP assembly, greatly increasing the optical absorption path. Secondly, the high porosity greatly decreases the filling ratio of metal (compared with film or other larger filling ratio structures), which decreases the effective refractive index as well as surface reflectance. Thirdly, the highly porous structure combined with proper surface wettability makes the entire structure self-floatable on the water surface, further reducing the thermal loss to underlying bulk water. Therefore, it provides point-of-use design rules for highly efficient solar evaporators, which includes efficient anti-reflectivity [94, 95], high density of optical modes [96, 97], and strong light coupling and scattering channels for efficient absorption with well-defined porous structure. In their work, the porous substrate provided an impedance match for efficient antireflection and strong light coupling to the optical modes, acting as an efficient light trapper by strongly scattering the incident light into the nanopores. The randomly sized and distributed metal NPs in these pores enabled a high density of hybridized localized surface plasmon resonance to absorb a wide wavelength range of light efficiently.

Based on the above design principles, the Zhu group has also explored optimal cost-effective three-dimensional aluminum NPs (Figure 4B–D) [98, 99]. By combining the plasmonic hybridization effect, porous substrate effect, the intrinsic self-limiting oxidation effect, and intrinsic aluminum absorption in the NIR region (~800 nm), the Al/AAO absorber enabled an efficient solar absorption up to 96.5% (Figure 4E), beneficial for highly efficient solar evaporation when combined with other advantages mentioned above.

Apart from the complex hybridization of different plasmonic resonant modes to increase the light absorption mentioned above, a novel broadband absorber made of self-assembled tellurium (Te) NPs with a wide size distribution was designed by the Yang group, combining both plasmonic-like and all-dielectric Mie-type resonances [87]. Perfect absorption (more than 85%) was achieved in the entire spectrum of solar radiation (300–2000 nm), derived from the unique optical duality of Te NPs. They discovered that the real part of permittivity of Te transforms from negative to positive at the UV-vis-NIR region, which endows Te NPs with optical duality. The Te NP gradually converts from a plasmonic-like material to a high-index all-dielectric material, as the size increases from 10 to 300 nm. Both the plasmonic-like and Mie-type resonances strongly extend and enhance optical absorption. It was the first reported material that can exhibit optical duality in the solar radiation region. Therefore, their findings demonstrated that the non-noble metal Te NPs could be a promising nanophotonic material for solar energy absorption, and provided insight into perfect absorption assisted by various optical modes.

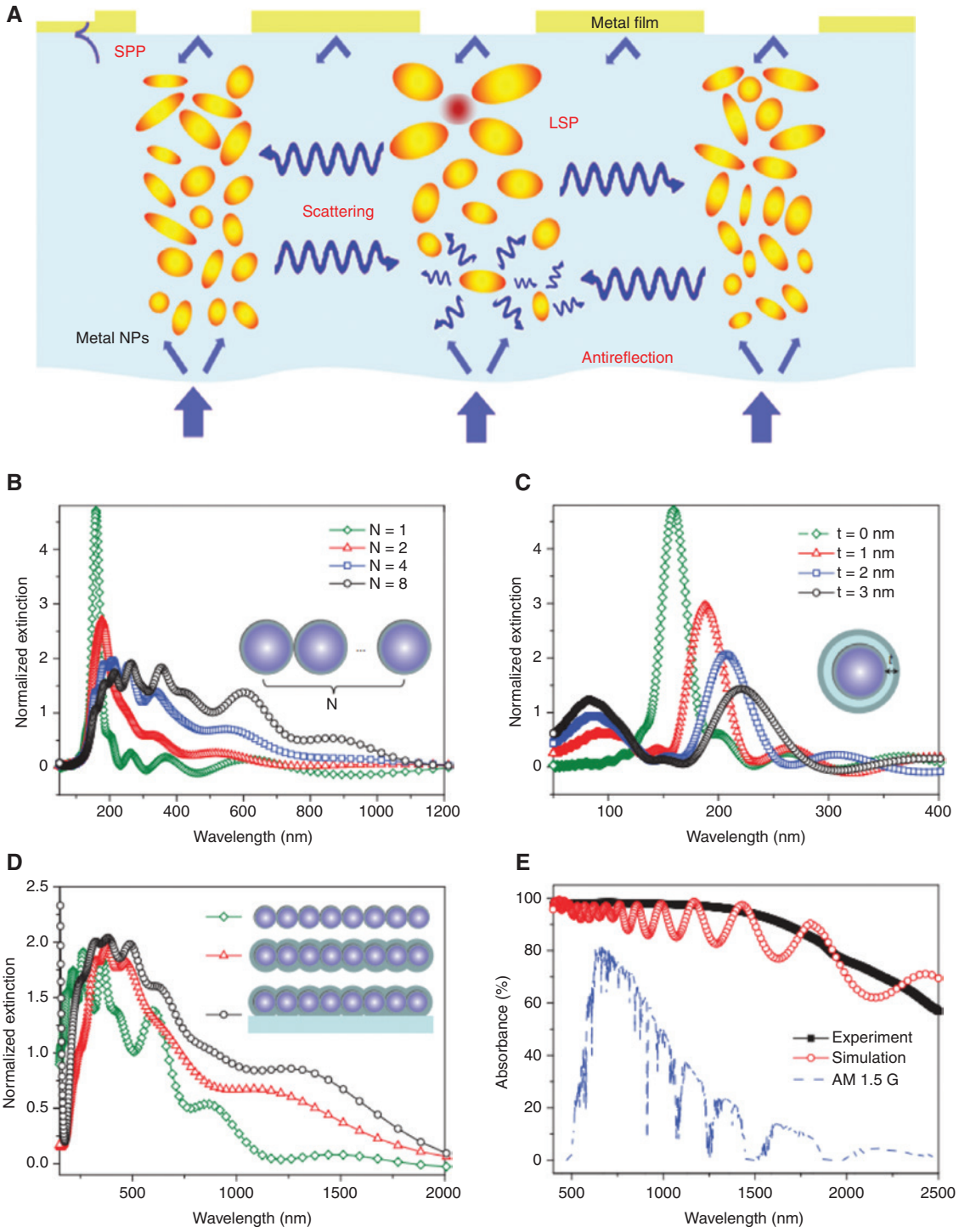

Figure 4: (A) Schematic of hybridized plasmonic structure to enhance solar absorption [60]; dependence of calculated normalized extinction cross-section of Al nanoparticles on (B) the particle number N, (C) on the thickness of the alumina oxidation layer t, and (D) on the substrate; and (E) experimental and simulated absorption of aluminum-based plasmonic absorbers. The normalized spectral solar irradiance density of air mass 1.5 global (AM 1.5 G) tilt solar spectrum is shown by the blue dashed line [85]. (A) Adapted by permission from Ref. [60]. Copyright 2016 American Association for the Advancement of Science. (B)–(E) Reprinted with permission from Ref. [85]. Copyright 2016 Nature Publishing Group.

3.2 Heat localization for solar evaporation

For the entire solar evaporation process, light absorption is merely the first step; light-to-heat conversion is the second most important issue. Heat localization is widely regarded as one of the most crucial components of high efficiency SVGs, which can be enabled by both material/structure design and system design for plasmon-based solar evaporators.

From the material/structure level, heat localization can be enabled by plasmonic near-field enhancement, called optical induced thermal concentration. Once the energy of the incident light converts to the oscillation energy of free electrons, there will be different passageways: electron-to-photon, electron-to-electron, and electron-to-phonon, respectively, as illustrated in Figure 5A. In the first 1–100 fs following Landau

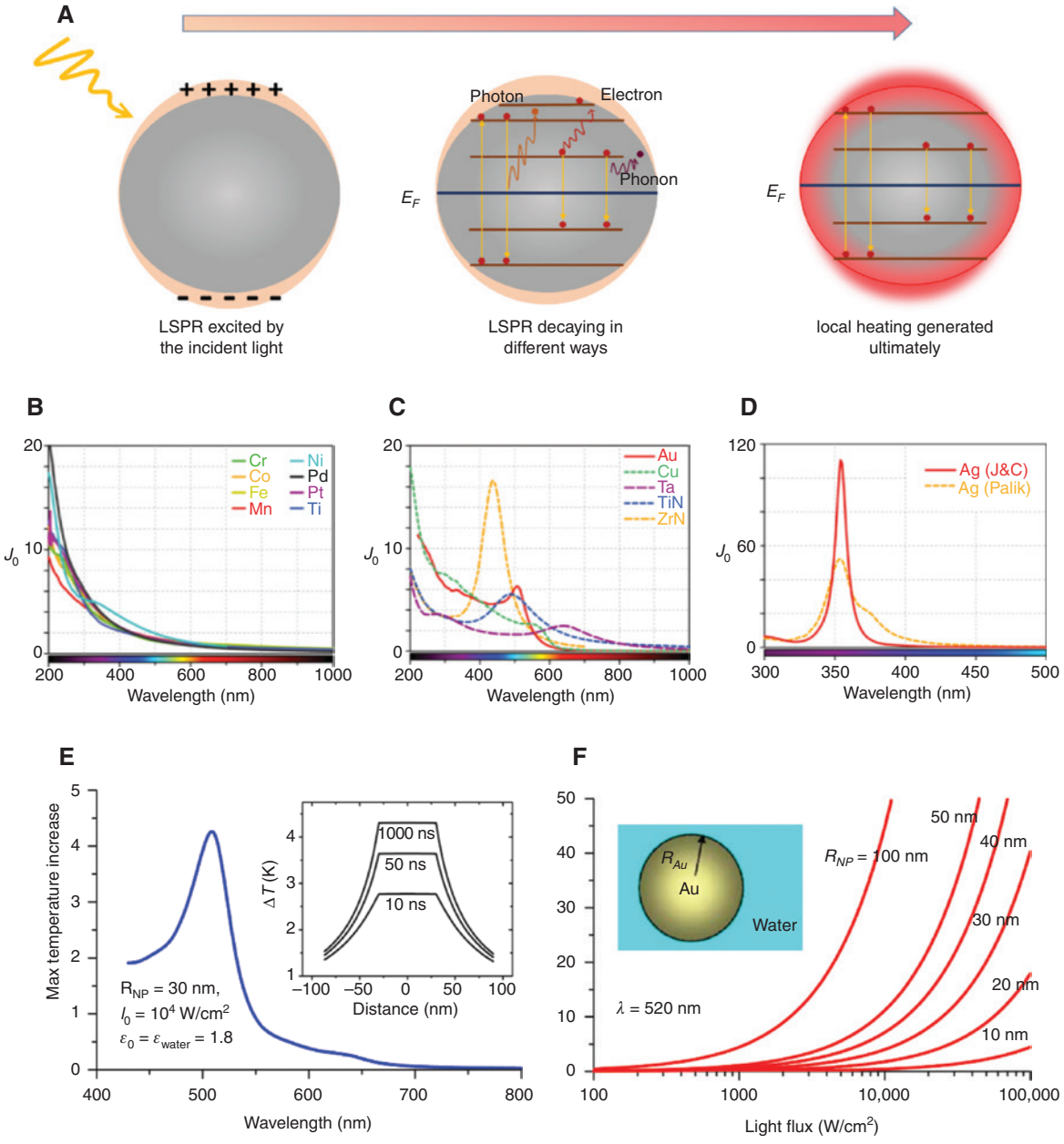

Figure 5: Plasmonic heat generation.
(A) Schematic of local heat generation process; (B)–(D) the comparison of Joule parameter for different materials [65]; (E) and (F) the calculated localized heating at the surface of Au NPs in the water for different incident light wavelength, distance (E) (inset: spatial distribution of temperature at different times) and the particle size (F) [25]. (B)–(D) Reprinted with permission from Ref. [65]. Copyright 2015 American Chemical Society. (E) and (F) Reprinted with permission from Ref. [25]. Copyright 2006 Springer.

damping, the thermal distribution of electron-hole pairs decays either through re-emission of photons or through carrier multiplication caused by electron-electron interactions. The hot carriers will redistribute their energy by electron-electron scattering processes on a time scale ranging from 100 fs to 1 ps. Finally, heat is transferred to the surroundings of the metallic structure on a longer time scale ranging from 100 ps to 10 ns, via thermal conduction [24]. As the enhanced electromagnetic field is localized, the generated heat is localized as well, which is beneficial for the evaporation of the liquid around the plasmonic materials.

To quantify the role of light-induced heat concentration of plasmonic materials to efficient photothermal conversion (solar evaporation), the dimensionless parameter Joule number $J_0\left(J_0=\frac{e\varepsilon''}{n_s}|E_{in}/E_0|^2\right)$ was introduced by Guillaume Baffou et al. [65]. This parameter contained the imaginary part of the permittivity of the material (ε''), and a large value of ε'' is beneficial for the photothermal conversion. As they considered the relation $qV=\sigma_{abs}I$ (q being the heat source density within the material, and I the light irradiance) the Joule parameter definition also had another equivalent expression: $J_0=\frac{\lambda_{ref}\sigma_{abs}}{2\pi V}$, in which λ_{ref} is about 1240 nm, σ_{abs} is the absorption cross section of the NPs, and V is the volume of the NP. They calculated the J_0 of some typical metals as plotted in Figure 5B–D. For a given material, J_0 is only related to the nature of the material, and therefore it offers a convenient reference tool for selecting the appropriate photothermal plasmonic materials. Among the most common plasmonic materials, gold is surprisingly not the largest; silver shows a much better potential for heat generation. In practice, however, silver NPs are highly prone to oxidation and aggregation under exposure to solar light. Another issue would be their application in the desalination process, where the presence of chloride anions would react with silver. Aluminum is also an ideal candidate for plasmonic photothermal applications due to its strong plasmon resonance in the UV range. However, the calculation might not be in accordance with experimental results because of the instability of metal surface similar for silver, as mentioned above [100–102]. What's more, the ability of heat generation also strongly connects with the incident light and the geometry factors as illustrated in Figure 5E and F [25]. In order to achieve a visible heating effect, NPs of relatively large radius (>10 nm) should be used [23, 25].

In the past years, two types of material/structure-induced heat localization have emerged. The first one is plasmonic nanofluid under certain conditions (Figure 6A and B). For the typical bulk heating system where the NPs are dispersed in liquid, heat localization can be achieved by fine-tuning the particle concentration. As demonstrated Ref. [103], there are three distinct regimes for plasmonic nanofluid-based solar evaporation. At low concentration or small volumes (Regime I), NPs serve as absorbers instead of scatterers, and Beer-Lambert law works in this regime. Therefore, all scattered photons are lost from the beam, and light transmits through the solution. Because of the linear relationship between particle concentration and absorption efficiency, the linear dependence on particle concentration in the log scale profile is presented. For higher concentrations (or multiple scattering regime, Regime II) where scattering length is comparable to characteristic dimensions of the nanofluid, NPs serve as both scatterers and absorbers. In this case, multiple scattering plays a crucial role and increases the average path length of the photons, which increases the absorption coefficient and concentrates light into a smaller penetration depth. Furthermore, at extremely high NP concentration (Regime III), photon absorption is saturated, and part of the incident photon will be back scattered off the fluid surface (Figure 6B). Note that plasmonic nanofluid in both Regimes I and III will encounter tremendous heat loss due to large optical and thermal dissipation. Regime II can be regarded as an interfacial-like solar evaporation by heating an infinite volume of bulk water, which has inspired the second type of plasmonic structure-induced local heating systems.

Unlike the plasmonic nanofluid system, the second type is featured by integrated structures hosted by thin porous substrates [55, 60, 85]. Such solar evaporators are self-floating on air/water interfaces due to their hydrophobic surface and/or low density [39, 40, 54, 105]. Suppressed thermal dissipation is commonly suggested due to the reduced effective thermal conductivity. Figure 6C and D illustrates one of the representative integrated plasmonic evaporators with material/structure-induced heat localization [85]. By assembling the close-packed metal NPs in a highly porous substrate, the evaporator can integrate in one structure the interfacial effects of self-floating substrates, as well as the NP-induced near-field enhancement effects as in nanofluids (Figure 6C). This leads to a suppressed heat dissipation to bulk water and thus a distinct temperature difference between vapor and underneath water (Figure 6D). Note that the thermal conductance loss for the material/structure designed system is still distinct due to direct contact between plasmonic materials and bulk water, especially for low solar irradiance. Researchers have been attempting to further decrease thermal conductance loss by introducing thicker thermal insulating layers into the plasmonic absorbers,

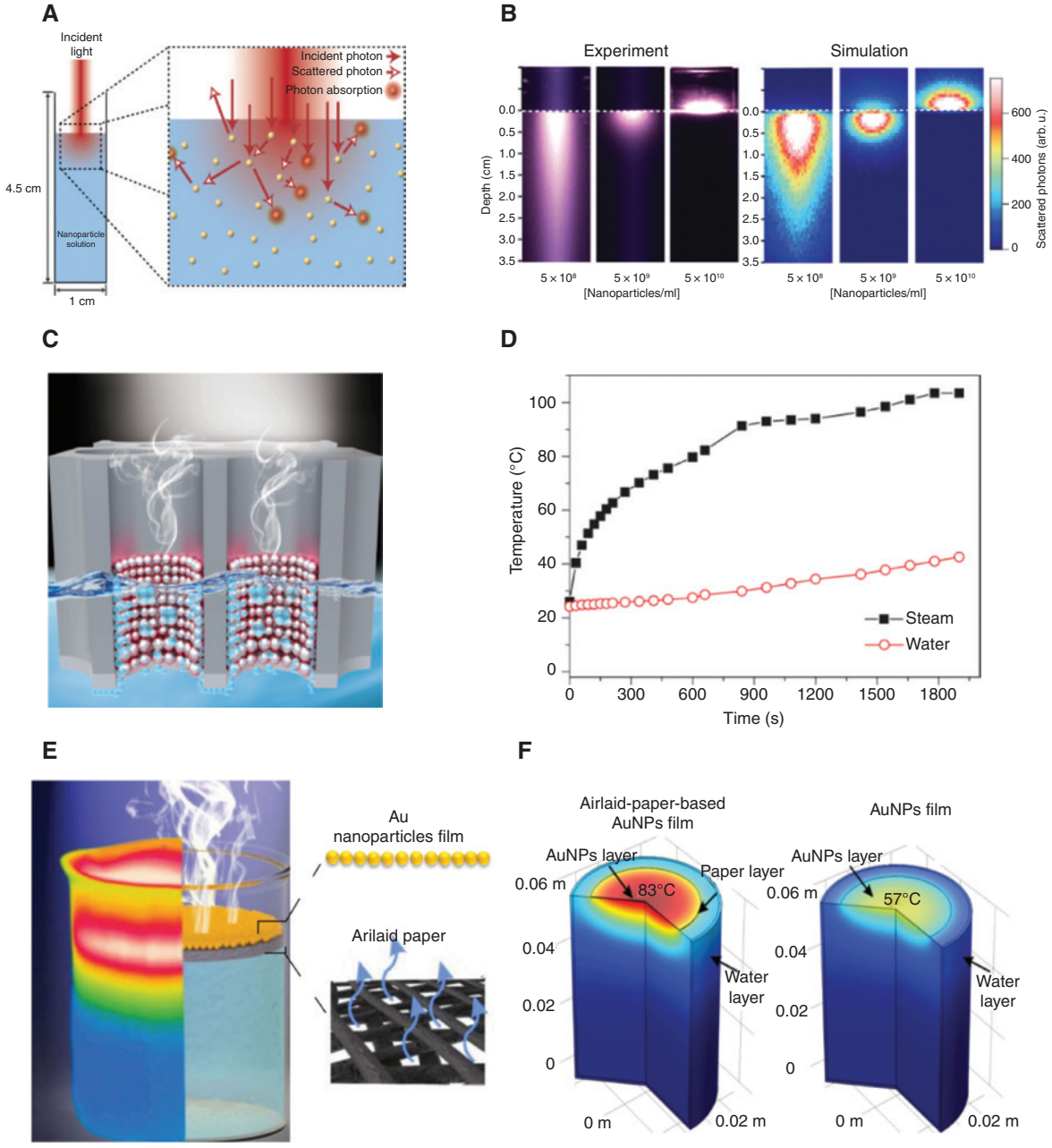

Figure 6: Heat localization.
(A) SiO_2/Au nanoparticles immersed in water and (B) three regimes of light propagation through the NPs colloid, depending on the NPs concentration [103]; (C) schematics of the self-floated solar evaporator based on the assembly Al nanoparticles on porous AAO membrane and (D) temperature changes of the steam and water over time (24°C ambient temperature and 48% humidity) [85]; (E) schematic illustration of the structure of air-laid paper-based gold nanoparticles (Au NPs) film evaporation system and (F) the simulated temperature distribution comparison of air-laid paper-based Au NPs film evaporation system with maximum temperature of 83°C and free-floating Au NP film with maximum temperature of 57°C [104]. (A) and (B) Reprinted with permission from Ref. [103]. Copyright 2014 American Chemical Society. (C) and (D) Reprinted with permission from Ref. [85]. Copyright 2016 Nature Publishing Group. (E) and (F) Reprinted with permission from Ref. [104].

such as porous membrane [61, 106], air-laid paper [54, 56], wood [59], and biofoam [57].

One of the representatives is the double-layer solar evaporators constructed with gold film/air-laid paper reported by the Deng group (Figure 6E), which can be regarded as a local heating design from the system level. Note that the average absorption efficiency of the gold film (with uniform gold particles of diameter ~17.4 ± 0.3 nm) is ~84% in 400–800 nm and the solar thermal efficiency reaches 77.8% under 4.5 Sun illumination [104]. It indicates

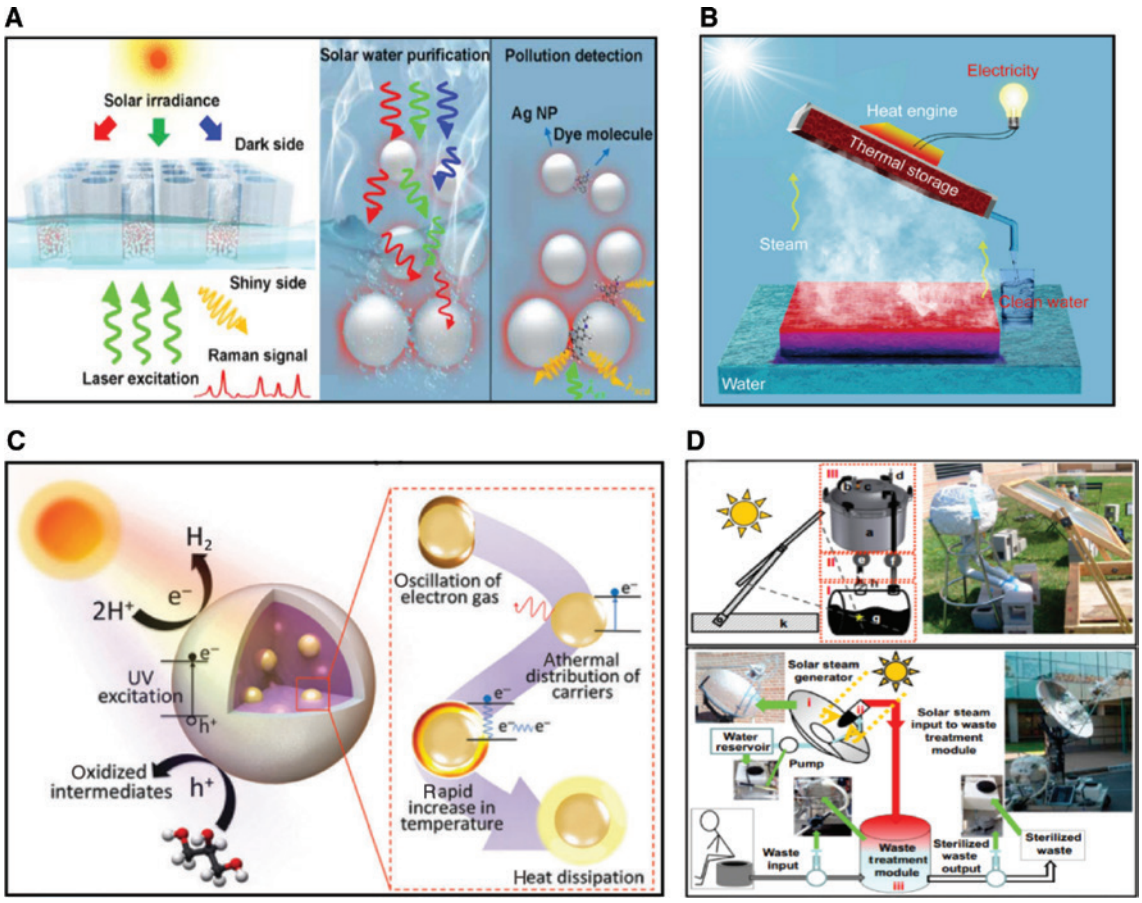

Figure 7: Dual-functional applications of plasmon-enhanced solar evaporation.
(A) Asymmetric plasmonic structures for solar water purification and pollution detection [107]; (B) clean water collection accompanied by the electric energy generation [108]; (C) SiO_2/Ag core-TiO_2 shell nanoparticles structures for both clean water generation and photo-catalysis [19]; (D) autoclave sterilization through high-temperature steam [58]. (A) Reprinted from Ref. [107]. Copyright 2018, with permission from Elsevier. (B) Reprinted from Ref. [108]. Copyright 2018, with permission from Elsevier. (C) Reprinted from Ref. [19]. (D) Reprinted from Ref. [58] Copyright 2013 National Academy of Sciences.

that, apart from the explanations from the optical viewpoint as suggested in [104], the unique textile-like porous hydrophilic paper enhances light absorption and reduces thermal conductance with the bulk water at the same time, which may play a crucial role for the highly efficient evaporation.

4 Applications

As illustrated above, plasmonic nanostructures with rational designs can achieve efficient and broadband absorption and heat localization and therefore enable efficient solar evaporation (with over 80% energy conversion efficiency commonly achieved). The evaporation with solar energy as the only energy input and high energy conversion efficiency has liad down a solid foundation to the exploitation of various applications. For example, Zhou et al. demonstrated the first plasmon-enhanced solar desalination device [60]. Their structure contains a nanoporous AAO membrane into which aluminum NPs are randomly dispersed. The as-prepared structure enabled a steam generation efficiency of 88.4% under 4 Sun illumination, and the produced clean water has salinity ~4 orders of magnitude lower than that of water sources. Ever since, there have been significant efforts to explore other choices of materials and designs of structures, to produce drinkable water with higher efficiency and lower cost.

Besides solar desalination, other practical functionalities can be integrated into the plasmonic structures. As an example, Chen et al. demonstrated an asymmetric plasmonic structure with dual functions, solar water purification, and pollution detection as illustrated in Figure 7A [107]. After the self-assembly of close-packed silver NPs into porous templates, the plasmonic structures showed different colors for the two sides. The dark porous side of the structure enabled efficient solar steam

generation (with energy transfer efficiency ~80%), while the shiny metallic side could enable sensitive chemicals detection using the surface enhanced Raman scattering effect, realizing a detection limit down to ~10^{-12} M. The dual functional structure could purify water and enable on-site pollution detection at the same time.

Another notable example is plasmonic structures designed by Gao Minmin et al. [19], which could enable water evaporation and fuel generation by water splitting. The structure took the form of a SiO_2 core embedded with Ag NPs and TiO_2 shells as depicted in Figure 7C. The TiO_2 shell coated by sol-gel method took in higher-energy photons for electron-hole pair generation, and the SiO_2/Ag core absorbs the lower energy photons for heat generation. Therefore, the integrated NPs offer both distillation production and clean fuel generation.

Solar steam of high temperature can enable various important applications beyond conventional low-temperature solar evaporation, such as sterilization, as plasmonic NPs can enable a fast responsive, high-temperature steam generation process. The pioneer work was conducted by the Halas group, where gold nanoshells were dispersed into water as shown in Figure 7D [58]. An equilibrium temperature of 140°C could be readily accomplished, a fatal environment for multiple bacteria sources. A closed-loop autoclave and an open-loop disposal system were subsequently designed to sterilize medical equipment and treat domestic solid waste, both of which survived the test of *Geobacillus stearothermophilus* elimination, indicating a successful sterilization cycle.

Note that, in most of the previously reported solar evaporation-based applications, heat (enthalpy) out of the solar steam is typically wasted to the environment. Recently, Li et al. reported a creative system which can store the generated latent heat enthalpy, even during night hours, providing an insightful initiative in the recycling of energy as demonstrated in Figure 7B [108]. Enthalpy recycling can be a promising direction for the optimization of vapor generation systems, to bridge the gap between solar steam generation and other heat-driven systems and energy-consuming fields.

5 Summary and outlook

In this review, we summarize various strategies for rational designs of plasmonic nanostructures for efficient solar evaporation, through enhanced light absorption and localized heating, and list out related potential applications. Despite tremendous progress, there are still issues and challenges that need to be addressed from both perspectives of fundamental understanding and practical applications. For example, it is still a challenge to precisely calibrate the temperature and thermal dynamics at nanoscale for the complicated photothermal processes. Moreover, the large-scale practical applications of desalination or water treatment call for not only more cost-effective materials and scalable processes, but also materials/structures with long-term chemical and physical stability. In addition, for high-temperature solar vapor applications, such as sterilization and electricity generation, it is urgent to develop spectrum-selective plasmonic absorbers with well-defined absorption spectra in both solar spectrum and mid-IR regime, in order to minimize heat losses of thermal radiation [109–111]. Actually, there is still a long way towards ideal plasmonic solar evaporators that possess simultaneous spectrum manipulation with optimized thermal and/or water transport system designs. Although further understandings and advancements are needed, the intrinsic advantages of plasmonic nanostructures with strong light-matter interactions and localized field make them promising candidates for solar evaporation and various other solar thermal applications.

Acknowledgements: We acknowledge the micro-fabrication center of National Laboratory of Solid State Microstructures (NLSSM) for technique support and Jiangsu Donghai Silicon Industry Science and Technology Innovation Center. This work is jointly supported by the National Key Research and Development Program of China (No. 2017YFA0205700) and the State Key Program for Basic Research of China (No. 2015CB659300), National Natural Science Foundation of China (Nos. 11874211, 11574143, 21805132, 11621091, 61735008), Natural Science Foundation of Jiangsu Province (Nos. BK20180341) and the Fundamental Research Funds for the Central Universities (Nos. 021314380140, 021314380150).

References

[1] Mezeme ME, Brosseau C. Engineering nanostructures with enhanced thermoplasmonic properties for biosensing and selective targeting applications. Phys Rev E 2013;87:012722.
[2] Jain PK, Huang X, Elsayed IH, Elsayed MA. Noble metals on the nanoscale: optical and photothermal properties and some applications in imaging, sensing, biology, and medicine. Acc Chem Res 2008;41:1578–86.
[3] Manjavacas A, Liu JG, Kulkarni V, Nordlander P. Plasmon-induced hot carriers in metallic nanoparticles. ACS Nano 2014;8:7630–8.
[4] Boltasseva A, Atwater HA. Low-loss plasmonic metamaterials. Science 2011;331:290–1.
[5] Koenderink AF, Alù A, Polman A. Nanophotonics: shrinking light-based technology. Science 2015;348:516–21.

[6] Hao E, Li S, Bailey RC, Zou S, Schatz GC, Hupp JT. Optical properties of metal nanoshells. J Phys Chem B 2004;108:1224–9.
[7] Bohren CF. How can a particle absorb more than the light incident on it? Am J Phys 1983;51:323–7.
[8] Schuller JA, Barnard ES, Cai W, Jun YC, White JS, Brongersma ML. Plasmonics for extreme light concentration and manipulation. Nat Mater 2010;9:193.
[9] Shen X, Cui TJ, Martin-Cano D, Garcia-Vidal FJ. Conformal surface plasmons propagating on ultrathin and flexible films. Proc Natl Acad Sci USA 2013;110:40–5.
[10] Wang Y, Plummer EW, Kempa K. Foundations of plasmonics. Adv Phys 2011;60:799–898.
[11] Prodan E, Radloff C, Halas NJ, Nordlander P. A hybridization model for the plasmon response of complex nanostructures. Science 2003;302:419–22.
[12] Oulton RF, Sorger VJ, Zentgraf T, et al. Plasmon lasers at deep subwavelength scale. Nature 2009;461:629–32.
[13] Bozhevolnyi SI, Erland J, Leosson K, Skovgaard MW, Hvam RM. Waveguiding in surface plasmon polariton band gap structures. Phys Rev Lett 2001;86:3008–11.
[14] Schmidt MA, Sempere LNP, Tyagi HK, Poulton CG, Russell PSJ. Waveguiding and plasmon resonances in two-dimensional photonic lattices of gold and silver nanowires. Phys Rev B 2008;77:033417.
[15] Yokogawa S, Burgos SP, Atwater HA. Plasmonic color filters for CMOS image sensor applications. Nano Lett 2012;12:4349–54.
[16] Chen Q, Cumming DRS. High transmission and low color cross-talk plasmonic color filters using triangular-lattice hole arrays in aluminum films. Opt Express 2010;18:14056–62.
[17] Liu N, Mesch M, Weiss T, Hentschel M, Giessen H. Infrared perfect absorber and its application as plasmonic sensor. Nano Lett 2010;10:2342–8.
[18] Sterl F, Strohfeldt N, Walter R, Griessen R, Tittl A, Giessen H. Magnesium as novel material for active plasmonics in the visible wavelength range. Nano Lett 2015;15:7949–55.
[19] Gao M, Connor PKN, Ho GW. Plasmonic photothermic directed broadband sunlight harnessing for seawater catalysis and desalination. Energy Environ Sci 2016;9:3151–60.
[20] Jiang N, Zhuo X, Wang J. Active plasmonics: principles, structures, and applications. Chem Rev 2018;118:3054–99.
[21] Atwater HA, Polman A. Plasmonics for improved photovoltaic devices. Nat Mater 2010;9:205–13.
[22] Jia B, Chen X, Saha JK, et al. Concept to devices: from plasmonic light trapping to upscaled plasmonic solar modules. Photonics Res 2013;1:22–7.
[23] Govorov AO, Richardson HH. Generating heat with metal nanoparticles. Nano Today 2007;2:30–8.
[24] Brongersma ML, Halas NJ, Nordlander P. Plasmon-induced hot carrier science and technology. Nat Nanotechnol 2015;10:25–34.
[25] Govorov AO, Zhang W, Skeini T, Richardson H, Lee J, Kotov NA. Gold nanoparticle ensembles as heaters and actuators: melting and collective plasmon resonances. Nanoscale Res Lett 2006;1:84–90.
[26] Hao J, Zhou L, Qiu M. Nearly total absorption of light and heat generation by plasmonic metamaterials. Phys Rev B 2011;83:165107.
[27] Brinson BE, Lassiter JB, Levin CS, Bardhan R, Mirin N, Halas NJ. Nanoshells made easy: improving Au layer growth on nanoparticle surfaces. Langmuir 2008;24:14166–71.
[28] Gobin AM, Lee MH, Halas NJ, James WD, Drezek RA, West JL. Near-infrared resonant nanoshells for combined optical imaging and photothermal cancer therapy. Nano Lett 2007;7:1929–34.
[29] Pissuwan D, Valenzuela SM, Cortie MB. Therapeutic possibilities of plasmonically heated gold nanoparticles. Trends Biotechnol 2006;24:62–7.
[30] Jain PK, El-Sayed IH, El-Sayed MA. Au nanoparticles target cancer. Nano Today 2007;2:16.
[31] Stern JM, Stanfield J, Kabbani W, Hsieh JT, Cadeddu JA. Selective prostate cancer thermal ablation with laser activated gold nanoshells. J Urol 2008;179:748–53.
[32] Alkilany AM, Thompson LB, Boulos SP, Sisco PN, Murphy CJ. Gold nanorods: their potential for photothermal therapeutics and drug delivery, tempered by the complexity of their biological interactions. Adv Drug Deliv Rev 2012;64:190–9.
[33] Gormley AJ, Larson N, Sadekar S, Robinson R, Ray A, Ghandehari H. Guided delivery of polymer therapeutics using plasmonic photothermal therapy. Nano Today 2012;7:158–67.
[34] Boyer D, Tamarat P, Maali A, Lounis B, Orrit M. Photothermal imaging of nanometer-sized metal particles among scatterers. Science 2002;297:1160–3.
[35] Righini M, Zelenina AS, Girard C, Quidant R. Parallel and selective trapping in a patterned plasmonic landscape. Nat Phys 2007;3:477–80.
[36] Liu G, Xu J, Wang K. Solar water evaporation by black photothermal sheets. Nano Energy 2017;41:269–84.
[37] Fang Z, Zhen YR, Neumann O, et al. Evolution of light-induced vapor generation at a liquid-immersed metallic nanoparticle. Nano Lett 2013;13:1736–42.
[38] Polman A. Solar steam nanobubbles. ACS Nano 2013;7:15–8.
[39] Zeng Y, Yao JF, Horri BA, et al. Solar evaporation enhancement using floating light-absorbing magnetic particles. Energy Environ Sci 2011;4:4074–8.
[40] Chen R, Wu Z, Zhang T, Yu T, Ye M. Magnetically recyclable self-assembled thin films for highly efficient water evaporation by interfacial solar heating. Rsc Adv 2017;7:19849–55.
[41] Li X, Xiao D, Zhang Z. Landau damping of quantum plasmons in metal nanostructures. New J Phys 2013;15:23011–25.
[42] Hedayati MK, Faupel F, Elbahri M. Tunable broadband plasmonic perfect absorber at visible frequency. Appl Phys A 2012;109:769–73.
[43] Kinkhabwala A, Yu Z, Fan S, Avlasevich Y, Müllen K, Moerner WE. Large single-molecule fluorescence enhancements produced by a bowtie nanoantenna. Nat Photonics 2009;3:654–7.
[44] Wu C, Neuner B III, Shvets G, et al. Large-area, wide-angle, spectrally selective plasmonic absorber. Phys Rev B Condens Matter 2011;84:173–7.
[45] Wu C, Neuner B III, John J, et al. Metamaterial-based integrated plasmonic absorber/emitter for solar thermo-photovoltaic systems. J Opt 2012;14:24005–011.
[46] Zhou L, Zhuang S, He C, Tan Y, Wang Z, Zhu J. Self-assembled spectrum selective plasmonic absorbers with tunable bandwidth for solar energy conversion. Nano Energy 2017;32:195–200.
[47] Wang J, Fan C, Ding P, et al. Tunable broad-band perfect absorber by exciting of multiple plasmon resonances at optical frequency. Opt Express 2012;20:14871–8.
[48] Chen H, Shao L, Li Q, Wang J. Gold nanorods and their plasmonic properties. Chem Soc Rev 2013;42:2679–724.
[49] Aydin K, Ferry VE, Briggs RM, Atwater HA. Broadband polarization-independent resonant light absorption using ultrathin plasmonic super absorbers. Nat Commun 2011;2:517.

[50] Ji C, Lee KT, Xu T, et al. Engineering light at the nanoscale: structural color filters and broadband perfect absorbers. Adv Opt Mater 2017;5:1700368.
[51] Toussaint KC Jr, Roxworthy BJ, Michaud S, Chen H, Bhuiya AM, Ding Q. Plasmonic nanoantennas: from nanotweezers to plasmonic photography. Opt Photonics News 2015;26:24–31.
[52] Neumann O, Urban AS, Day J, Lal S, Nordlander P, Halas NJ. Solar vapor generation enabled by nanoparticles. ACS Nano 2013;7:42–9.
[53] Swartz ET, Pohl RO. Thermal boundary resistance. Rev Mod Phys 1989;61:605–68.
[54] Wang Z, Liu Y, Tao P, et al. Bio-inspired evaporation through plasmonic film of nanoparticles at the air-water interface. Small 2014;10:3234–9.
[55] Liu Y, Lou J, Ni M, et al. Bioinspired bifunctional membrane for efficient clean water generation. ACS Appl Mater Interface 2016;8:772–9.
[56] Fang J, Liu Q, Zhang W, et al. Ag/diatomite for highly efficient solar vapor generation under one-sun irradiation. J Mater Chem A 2017;5:17817–21.
[57] Jiang Q, Tian L, Liu KK, et al. Bilayered biofoam for highly efficient solar steam generation. Adv Mater 2016;28:9400–7.
[58] Neumann O, Feronti C, Neumann AD, et al. Compact solar autoclave based on steam generation using broadband light-harvesting nanoparticles. Proc Natl Acad. Sci USA 2013;110:11677–81.
[59] Zhu M, Li Y, Chen F, et al. Plasmonic wood for high-efficiency solar steam generation. Adv Energy Mater 2018;8:1701028.
[60] Zhou L, Tan Y, Ji D, et al. Self-assembly of highlyefficient, broadband plasmonic absorbers for solar steam generation. Sci Adv 2016;2:e1501227.
[61] Wang X, He Y, Liu X, Cheng G, Zhu J. Solar steam generation through bio-inspired interface heating of broadband-absorbing plasmonic membranes. Appl Energy 2017;195:414–25.
[62] Gao M, Peh CK, Phan HT, Zhu L, Ho GW. Solar absorber gel: localizedmacro-nano heat channeling for efficient plasmonic au nanoflowers photothermicvaporization and triboelectric generation. Adv Energy Mater 2018;8:1800711.
[63] Gao M, Zhu L, Peh CK, Ho GW. Solar absorber material and system designs for photothermal water vaporization towards clean water and energy production. Energy Environ Sci 2019;12:841–64.
[64] Zhu L, Gao M, Peh CKN, Ho GW. Solar-driven photothermal nanostructured materials designs and prerequisites for evaporation and catalysis applications. Mater Horizons 2018;5:323–43.
[65] Lalisse A, Tessier G, Plain J, Baffou G. Quantifying the efficiency of plasmonic materials for near-field enhancement and photothermal conversion. J Phys Chem C 2015;119:25518–28.
[66] Link S, El-Sayed MA. Size and temperature dependence of the plasmon absorption of colloidal gold nanoparticles. J Phys Chem B 1999;103:4212–7.
[67] Wiley BJ, Chen Y, Mclellan JM, et al. Synthesis and optical properties of silver nanobars and nanorice. Nano Lett. 2007;7:1032–6.
[68] Zhu J, Li J-J, Zhao J-W. The effect of dielectric coating on the local electric field enhancement of Au-Ag core-shell nanoparticles. Plasmonics 2015;10:1–8.
[69] Hentschel M, Saliba M, Vogelgesang R, Giessen H, Alivisatos AP, Liu N. Transition from isolated to collective modes in plasmonic oligomers. Nano Lett 2010;10:2721–6.
[70] Lu X, Rycenga M, Skrabalak SE, Wiley B, Xia Y. Chemical synthesis of novel plasmonic nanoparticles. Annu Rev Phys Chem 2009;60:167–92.
[71] Long R, Li Y, Song L, Xiong Y. Coupling solar energy into reactions: materials design for surface plasmon-mediated catalysis. Small 2015;11:3873–89.
[72] Pastoriza-Santos I, Liz-Marzán LM. N,N-Dimethylformamide as a reaction medium for metal nanoparticle synthesis. Adv Funct Mater 2009;19:679–88.
[73] Grady NK, Halas NJ, Nordlander P. Influence of dielectric function properties on the optical response of plasmon resonant metallic nanoparticles. Chem Phys Lett 2004;399:167–71.
[74] Herrera LJM, Arboleda DM, Schinca DC, Scaffardi LB. Determination of plasma frequency, damping constant, and size distribution from the complex dielectric function of noble metal nanoparticles. J Appl Phys 2014;116:233105.
[75] Zoric I, Zach M, Kasemo B, Langhammer C. Gold, platinum, and aluminum nanodisk plasmons: material independence, subradiance, and damping mechanisms. ACS Nano 2011;5:2535–46.
[76] Liu N, Fu L, Guo H, Kaiser S, Schweizer H, Giessen H. Three-dimensional metamaterials at optical frequencies. In: Conference on Lasers & Electro-optics, 2008.
[77] Luk'yanchuk B, Zheludev NI, Maier SA, et al. The Fano resonance in plasmonic nanostructures and metamaterials. Nat Mater 2010;9:707–15.
[78] Shao L, Fang C, Chen H, Man Y, Wang J, Lin H. Distinct plasmonic manifestation on gold nanorods induced by the spatial perturbation of small gold nanospheres. Nano Lett 2012;12:1424–30.
[79] Lovera A, Gallinet B, Nordlander P, Martin OJ. Mechanisms of Fano resonances in coupled plasmonic systems. ACS Nano 2013;7:4527–36.
[80] Shafiei F, Monticone F, Le KQ, et al. A subwavelength plasmonic metamolecule exhibiting magnetic-based optical Fano resonance. Nat Nanotechnol 2013;8:95–9.
[81] Zhou L, Li X, Ni GW, Zhu S, Zhu J. The revival of thermal utilization from the sun: interfacial solar vapor generation. Natl Sci Rev 2019 (in press).
[82] Tian Y, Zhao CY. A review of solar collectors and thermal energy storage in solar thermal applications. Appl Energy 2013;104:538–53.
[83] Kuzyk A, Schreiber R, Zhang H, Govorov AO, Liedl T, Liu N. Reconfigurable 3D plasmonic metamolecules. Nat Mater 2014;13:862–6.
[84] Yang S, Ni X, Yin X, et al. Feedback-driven self-assembly of symmetry-breaking optical metamaterials in solution. Nat Nanotechnol 2014;9:1002–6.
[85] Zhou L, Tan Y, Wang J, et al. 3D self-assembly of aluminium nanoparticles for plasmon-enhanced solar desalination. Nat Photonics 2016;10:393–8.
[86] Peña-Rodríguez O, Revera A, Campoy-Quiles M, Pal U. Tunable Fano resonance in symmetric multilayered gold nanoshells. Nanoscale 2013;5:209–16.
[87] Ma C, Yan J, Huang Y, Wang C, Yang G. The optical duality of tellurium nanoparticles for broadband solar energy harvesting and efficient photothermal conversion. Sci Adv 2018;4:eaas9894.
[88] Bae K, Kang G, Cho SK, Park W, Kim K, Padilla WJ. Flexible thin-film black gold membranes with ultrabroadband plasmonic nanofocusing for efficient solar vapour generation. Nat Commun 2015;6:10103.
[89] Zielinski MS, Choi JW, La Grange T, et al. Hollow mesoporous plasmonic nanoshells for enhanced solar vapor generation. Nano Lett 2016;16:2159–67.

[90] Zhu H, Luo W, Ciesielski PN, et al. Wood-derived materials for green electronics, biological devices, and energy applications. Chem Rev 2016;116:9305–74.
[91] Xue G, Liu K, Chen Q, et al. Robust and low-cost flame-treated wood for high-performance solar steam generation. ACS Appl Mater Interfaces 2017;9:15052–7.
[92] Liu KK, Jiang Q, Tadepallifit S, et al. Wood-graphene oxide composite for highly efficient solar steam generation and desalination. ACS Appl Mater Interfaces 2017;9:7675–81.
[93] Søndergaard T, Novikov SM, Holmgaard T, et al. Plasmonic black gold by adiabatic nanofocusing and absorption of light in ultra-sharp convex grooves. Nat Commun 2012;3:969.
[94] Garcia-Vidal FJ, Pitarke JM, Pendry JB. Effective medium theory of the optical properties of aligned carbon nanotubes. Phys Rev Lett 1997;78:4289–92.
[95] Xi JQ, Schubert MF, Kim JK, et al. Optical thin-film materials with low refractive index for broadband elimination of Fresnel reflection. Nat Photonics 2007;1:176–9.
[96] Yu Z, Raman A, Fan S. Fundamental limit of nanophotonic light trapping in solar cells. Proc Natl Acad Sci USA 2010;107:17491–6.
[97] Chou JB, Yeng YX, Lee YE, et al. Enabling ideal selective solar absorption with 2D metallic dielectric photonic crystals. Adv Mater 2014;26:8041–5.
[98] Langhammer C, Schwind M, Kasemo B, Zoriä I. Localized surface plasmon resonances in aluminum nanodisks. Nano Lett 2008;8:1461–71.
[99] Knight MW, King NS, Liu L, Everitt HO, Nordlander P, Halas NJ. Aluminum for plasmonics. ACS Nano 2014;8:834–40.
[100] Mcmahon M, Lopez R, Meyer HM, Feldman LC, Haglund RF. Rapid tarnishing of silver nanoparticles in ambient laboratory air. Appl Phys B-Lasers O 2005;80:915–21.
[101] Guler U, Turan R. Effect of particle properties and light polarization on the plasmonic resonances in metallic nanoparticles. Opt Express 2010;18:17322–38.
[102] Bell AR, Fairfield JA, McCarthy EK, et al. Quantitative study of the photothermal properties of metallic nanowire networks. ACS Nano 2015;9:5551–8.
[103] Hogan NJ, Urban AS, Ayala-Orozco C, Pimpinelli A, Nordlander P, Halas NJ. Nanoparticles heat through light localization. Nano Lett 2014;14:4640–5.
[104] Liu Y, Yu S, Feng R, et al. A bioinspired, reusable, paper-based system for high-performance large-scale evaporation. Adv Mater 2015;27:2768–74.
[105] Hua Z, Li B, Li L, Yin X, Chen K, Wang W. Designing a novel photothermal material of hierarchical microstructured copper phosphate for solar evaporation enhancement. J Phys Chem C 2017;121:60–9.
[106] Zhang L, Xing J, Wen X, Chai J, Wang S, Xiong Q. Plasmonic heating from indium nanoparticles on a floating microporous membrane for enhanced solar seawater desalination. Nanoscale 2017;9:12843–9.
[107] Chen C, Zhou L, Yu J, et al. Dual functional asymmetric plasmonic structures for solar water purification and pollution detection. Nano Energy 2018;51:451–6.
[108] Li X, Min X, Li J, et al. Storage and recycling of interfacial solar steam enthalpy. Joule 2018;2:2477–84.
[109] Robitaille PM. On the validity of Kirchhoff's law of thermal emission. IEEE T Plasma Sci 2003;31:1263–7.
[110] Planck M. The theory of heat radiation. Appl Opt 1992;31:7161.
[111] Jiang D, Yang W, Tang A. A refractory selective solar absorber for high performance thermochemical steam reforming. Appl Energy 2016;170:286–92.